IEEE Control Systems Letters paper presented at
2023 62nd IEEE Conference on Decision and Control (CDC)
December 13-15, 2023. Marina Bay Sands, Singapore

Hybrid dynamical control for discharging rate consensus in AC-bus microgrids*

Maria Camila Merchan-Riveros[1], Carolina Albea[1]

***Abstract*— In this work, a robust distributed hybrid algorithm is proposed for the primary and secondary control loops of an island AC-bus microgrid to provide large-signal stability of the complete system. A secondary control loop is designed from droop control and multi-agent systems theory to ensure that the State Of Charge (SOC) of the batteries in discharging mode converges to a consensus. Furthermore, this distributed strategy ensures robustness with respect to any plug-and-play event or communication failure. The DC-AC power converter of each battery in discharging mode is controlled in the primary loop by using hybrid dynamical system theory, which considers non-trivial issues in the model (switching and affine terms) and in the signals (constraints in the dwell time). A suited selection of gains allows using singular perturbation analysis to provide large-signal stability properties for the complete nonlinear model.**

I. INTRODUCTION

The use of renewable energies can mitigate the effects of climate change. The concept of microgrids emerges as a promising solution to integrate renewable energy sources into the conventional electrical grid [1]. These systems are defined as electric energy systems composed of Distributed Generation (DG) units, Distributed Energy Storage (DES) systems and loads, which can be located at noteworthy distance.

DES systems, which are a set of Battery Energy Storage System (BESS), are usually installed close to loads and are more reliable and efficient than a single energy storage element, especially if they are combined with microgrids [2]. The importance of these DES systems is revealed when the microgrid works in islanded mode (i.e., non connected to the utility grid), since they must provide grid-forming generation.

Nowadays, the most costly elements in a microgrid from an economic and environmental point of view are the DES systems. For this reason, it is crucial to increase the lifespan of the batteries to reduce their degradation. It is known, that the battery degradation can be improved if they operate between 20% and 80% of their State Of Charge (SOC). A way to help guarantee this operation mode is to drive all the SOCs of the batteries to a consensus [3].

The literature provides some centralized, decentralized [4] and distributed [5] solutions to this problem. It is well known that distributed controllers, which follow the idea: *think globally, act locally* to get a consensus between the SOCs of the batteries, generate more reliable and scalable systems, and make this solution more attractive. In [6], the authors propose an improved droop control in AC microgrids based on frequency scheduling, using the average SOC value calculated from Multi-Agent Systems (MAS) to get a SOC consensus (a previous work was done in DC microgrids [5]). A similar approach was developed in [7]. The authors of [8] presented another distributed algorithm, which uses a nonlinear sliding-mode control law to locally steer the estimated SOC of each battery to a common reference, which is calculated by a fixed-time observer. In [3], a consensus algorithm in discharging mode where each battery communicate with all the other batteries was introduced. In general, either the control results in microgrids do not include the control loop of the power converters, or if they take into account the converter dynamics, global stability are not guaranteed or only limited to small signals. This lack of theoretical analysis diminishes the reliability and/or the efficiency of the microgrids [9].

The recent literature demonstrates the increasing interest of providing large-signal stability in microgrids. In particular, [10] highlights the need to consider the power converter dynamics and provide a large-signal stability analysis to reduce the undesirable effects that cause large disturbances. Moreover, this issue is also pointed out in [11], where the authors stress the problems caused by structural changes. Interestingly, a large-signal stability analysis was conducted for an AC microgrid in [12]. These works consider power converter dynamics, but they are limited by DC microgrids or microgrids without batteries, among other system reductions.

Consequently, it is necessary to get a large-signal stability property in a microgrid with DES system, considering the power converters that connect the batteries to the bus line.

The objectives of the paper are: 1) to ensure that the estimated SOCs of the set of batteries in discharging mode of the DES system in an islanded AC microgrid converge to a consensus in order to increase the battery lifespan and it is robust with respect to any plug-and-play event and any communication failure; 2) to design a

*This work was supported in part by the Ministerio de Ciencia e Innovación MCIN/AEI/10.13039/501100011033/ under Grant PID2019-105890RJ-I00 and Grant PID2019-109071RB-I00; in part by the Agence Nationale de la Recherche (ANR), France, under Grant "HISPALIS" ANR-18-CE40-0022-01; and in part by the Consejería de Transformación Económica, Industria, Conocimiento y Universidades de la Junta de Andalucía and by Fondos del Programa Operativo FEDER Andalucía under Grant P20_01116.

[1]The authors are with Department of Systems and Automatic Engineering, Escuela Superior de Ingenieros, University of Seville, 41092 Seville, Spain e-mail: mmriveros, albea@us.es

complete hybrid model that considers both the secondary and primary control loops; and 3) to provide a large-signal stability. To achieve these objectives, a control loop scheme is proposed, as depicted in Fig. 1. In the secondary loop is expected to achieve a consensus between the estimated SOCs, Ψ_i, of the batteries, which is reached through a consensus algorithm between the references of the neighboring estimated SOCs, $\Psi_{r,i}$, based on MAS that feeds the droop control. This last one generates the inverter references, $x_{r,i}$, and guarantees the convergence of Ψ_i and active power, P_i, to their references, $\Psi_{r,i}$ and $P_{r,i}$, respectively. Moreover, the primary loop is composed of the inner control loop of the power converter that leads to a hybrid non-linear system (due to the switches, the affine terms, and the constraints on the dwell times). The complete system is modeled as a hybrid dynamical system formulation [13], [14]. Previous research on power converter systems has proposed a hybrid framework [15], [16].

Notation: $\mathbb{R}$ is the set of real numbers. $\mathbb{R}^{n\times m}$ and $\mathbb{R}^n$ represent all the real $n \times m$ matrices and the n vectors, respectively. eig(M) represents the eigenvalue of the matrix M. Re(a) is the real part of the complex number a. I, $\mathbf{0}$ and $\mathbf{1}$ denote the identity matrix, column vectors of zeros and ones of suitable dimensions, respectively. $\emptyset$ represents an empty set. The Euclidean norm of the vector $x \in \mathbb{R}^n$ is denoted by $|x|$. For any symmetric matrix M of $\mathbb{R}^{n\times n}$, the notation $M \succ 0$ ($M \prec 0$) means that the eigenvalues of M are strictly positive (negative). $\underset{i\in\mathcal{N}}{\text{diag}}\{a_i\}$ and $\underset{i\in\mathcal{N}}{\text{col}}\{a_i\}$ are a diagonal matrix and a column vector, respectively, whose elements are $a_1, a_2, ..., a_N$.

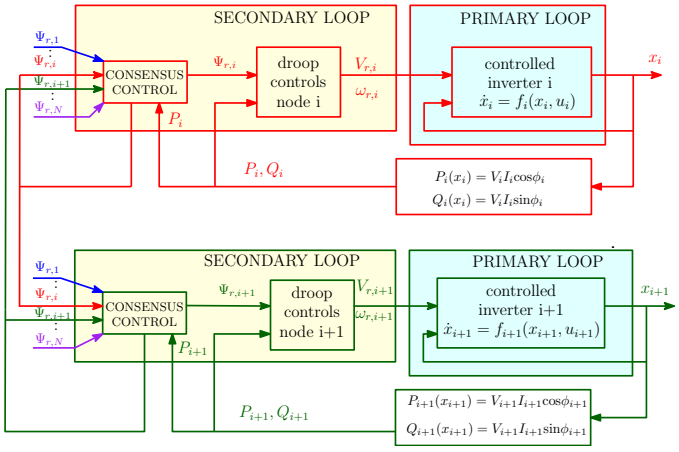

Fig. 1. Primary and secondary control loops in an islanded AC microgrid.

II. DYNAMIC MODELS IN THE PRIMARY ANS SECONDARY CONTROL LOOPS

This section describes the three dynamic models to get the following control objectives:

- Inverter control in the primary loop: convergence of state x_i to a small neighbourhood of $x_{r,i}$.
- Consensus algorithm in the secondary loop: convergence of Ψ_i to a consensus Ψ^*.
- Droop control in the secondary loop: convergence of Ψ_i and P_i to their references $\Psi_{r,i}$ and $P_{r,i}$.

A. Inverter model and control.

First, let us consider that the inverters that connect the batteries in discharging mode with the Point of Common Coupling (PCC) are half-bridge converters. The dynamical model of these inverters $i \in \mathcal{N} := [1, 2, ..., N]$ can be rewritten according to [15]

$$\begin{aligned} \dot{x}_i &= A_i x_i + B_i u_i \\ \dot{z}_i &= \Theta_i(\omega_{r,i}) z_i \\ \tilde{x}_i &= x_i - \Pi_i(\omega_{r,i}) z_i, \end{aligned} \tag{1}$$

where $A_i := \begin{bmatrix} -\frac{R_{LS,i}}{L_i} & -\frac{1}{L_i} \\ \frac{1}{C_i} & -\frac{1}{R_i C_i} \end{bmatrix}$, $B_i = \begin{bmatrix} \frac{V_{in,i}}{L_i} \\ 0. \end{bmatrix}$, $x_i = [i_{L,i}, v_{C,i}]^\top$ represents the state vector and u_i is the input control signal which switches in $\mathbb{K} := \{-1, 1\}$. $\omega_{r,i}$ and $V_{r,i}$ are the frequency and voltage reference, respectively, C_i and L_i are the capacitance and inductance respectively, R_i and $R_{LS,i}$ are the converter load and the parasitic resistance respectively, and $V_{in,i}$ the input voltage. $\Theta_i(\omega_{r,i}) = \begin{bmatrix} 0 & -\omega_{r,i} \\ \omega_{r,i} & 0 \end{bmatrix}$, $\Pi_i(\omega_{r,i}) := \begin{bmatrix} \omega_{r,i} C_i & \frac{1}{R_i} \\ 0 & 1 \end{bmatrix}$ and $z_i = [z_{i,1}, z_{i,2}]^\top \in \mathbb{R}^2$ models a generic oscillator, such that $z_{i,2} = V_{r,i} \sin(\omega_{r,i} t)$.

The error equation is formulated as follows

$$\begin{aligned} \dot{\tilde{x}}_i &= A_i \tilde{x}_i + B_i v_i \\ v_i &= u_i - \Gamma_i(\omega_{r,i}, V_{r_i}) z_i \in \mathbb{R}, \end{aligned} \tag{2}$$

with

$$\begin{aligned} z_i \in \Phi_i, \quad & \Phi_i := \{z_{1,i}, z_{2,i} \in \mathbb{R} : z_{1,i}^2 + z_{2,i}^2 = V_{r,i}^2\}, \\ v_i \in \Xi_i, \quad & \Xi_i := \{v_i = u_i - \Gamma_i z_i, u_i \in \mathbb{K}, z_i \in \Phi_i\}, \end{aligned}$$

$\Gamma_i := \begin{bmatrix} \frac{\omega_{r,i} L_i}{R_i V_{in,i}} + \frac{\omega_{r,i} R_{LS,i} C_i}{V_{in,i}} & \left(\frac{1}{L_i} - C_i \omega_{r,i}^2 + \frac{R_{LS,i}}{L_i R_i}\right) \frac{L_i}{V_{in,i}} \end{bmatrix}$.

Note that Γ_i, Θ_i and Π_i have been selected according to the output regulation problem defined in (1).

Assumption 1: [15] Consider model (1). For a given matrix $Q_{L,i} \succ 0 \in \mathbb{R}^{n\times n}$, there exists a matrix $P_{L,i} \succ 0 \in \mathbb{R}^{n\times n}$ such that

1) matrix A_i verifies

$$A_i^T P_{L,i} + P_{L,i} A_i + 2 Q_{L,i} \prec 0 \tag{3}$$

2) and, for any periodic signal $z(t) \in \mathbb{R}^n$ of period T_p, there exists a $\lambda_{j,e,i}(t)$ for each $j \in \mathbb{K}$ such that $\lambda_{-1,e,i}(t) + \lambda_{1,e,i}(t) = 1$ such that

$$\lambda_{1,e,i}(t) - \lambda_{-1,e,i} - \Gamma_i(\omega_{r,i}, V_{r_i}) z_i(t) = 0. \tag{4}$$

The Hurwitz requirement for matrices A_i is a common property in converter models [17], [15].

The control law used here for u_i will be the one given in the previous work [15] based on the "argmin" operator.

B. Consensus algorithm

A consensus algorithm for SOC references ($\Psi_{r,i}$) is proposed here according to

$$\dot{\Psi}_{r,i} = -K_c \sum_{j=1}^{N} (\Psi_{r,i} - \Psi_{r,j}) - K_e(\Psi_{r,i} - \Psi_i) \tag{5}$$

being K_c and K_e positive parameters. As in [3] the adopted estimation method of the SOC is considered to be $\dot{\Psi}_i = -\delta_i P_i$ with δ_i a constant that gathers the maximum capacity and efficiency of the battery. The intuitive idea of this expression is the following. The first term of (5) looks for achieving a consensus between all $\Psi_{r,i}$, while the second term collects the deviation between the estimated SOC of BESS$_i$, Ψ_i, and its reference $\Psi_{r,i}$. The next droop control is key to guarantee that the estimated SOC converges to its reference, tending this deviation to zero in a finite time, as will be proven later.

C. Droop control

A droop control is used here to guarantee that the estimated SOCs and active powers converge to their references, which are given by the consensus algorithm (5). This droop control adjusts the frequency and amplitude of the inverter voltage references, as follows.

$$\omega_{r,i} = \omega_n - \mathcal{K}_{d,1}(\Psi_i - \Psi_{r,i}) - \mathcal{K}_{d,2} \int (\Psi_i - \Psi_{r,i}) dt - \mathcal{K}_{d,3}(P_i - P_{r,i}) \tag{6}$$

$$V_{r,i} = V_n - K_{V,i} Q_i \tag{7}$$

where ω_n and V_n, are the nominal frequency and voltage, respectively. P_i and Q_i are the active and reactive powers. As seen in many references, this droop control guarantees that Ψ_i and P_i converge to their reference values $\Psi_{r,i}$ and $P_{r,i}$ respectively. [3], [6]. However, in in Section III we will prove that this convergence is asymptotically stable.

Finally, $\mathcal{K}_{d,1} := \frac{K_\omega}{K_1}$, $\mathcal{K}_{d,2} := \frac{K_\omega}{K_1}\left(K_\Psi + \frac{K_1^2}{K_\omega} + \frac{K_0^2}{K_P}\right)$, $\mathcal{K}_{d,3} := \frac{K_\omega K_0}{K_1 K_P}$, are the droop control gains, being $K_\omega, K_\Psi, K_P, K_0, K_1$ positive parameters, which are used later in the hybrid scheme.

III. HYBRID CONTROL STRUCTURE

The goal in this section is to propose a compact hybrid dynamical structure for the primary and secondary control levels, following the theory given in [14]. The dynamics of node i are collected in the scheme

$$\mathcal{H}_i : \begin{cases} \dot{\xi}_i &= f_i(\xi_i, \Psi_r) \qquad \xi_i \in \mathcal{C}_i \times [0,1] \\ \xi_i^+ &\in G_i(\xi_i) \qquad \xi_i \in \mathcal{D}_i \times [0,1] \end{cases} \tag{8}$$

being $\Psi_r := \underset{i\in\mathcal{N}}{\text{col}}\{\Psi_{r,i}\} \in [0,1]^N$, $\xi_i := [\xi_{1,i}^\top, \xi_{2,i}^\top, \Psi_{r,i}]^\top$ such that $\xi_{1,i} := [\tilde{\omega}_i, \tilde{\Psi}_i, \tilde{P}_i]^\top$ and $\xi_{2,i} := [\tilde{x}_i^\top, z_i, v_i, \tau_i]^\top$. Being $\tilde{\Psi}_i := \Psi_i - \Psi_{r,i}$, $\tilde{P}_i := P_i - P_{r,i}$, $\tilde{\omega}_i := \omega_{r,i} - \omega_{n,p,i}$ where $\omega_{n,p,i}$ is the nominal frequency associated with the operating point [6]. Therefore, it is defined by $\tilde{\omega}_{n,i} := \omega_{n,p,i} - \omega_n$. τ_i is a timer evolving in $[0,T]$ which is used to ensure a minimum-dwell time in the converter switching. f_i and G_i define a continuous-time dynamic map and a discrete-time dynamic (set-valued) map respectively, and they are:

$$f_i := \begin{bmatrix} -K_\omega \tilde{\omega}_i - K_1 \tilde{\Psi}_i \\ -K_\Psi \tilde{\Psi}_i + K_1 \tilde{\omega}_i + K_0 \tilde{P}_i \\ -K_P \tilde{P}_i - K_0 \tilde{\Psi}_i \\ \alpha_i (A_i \tilde{x}_i + B_i v_i) \\ \Theta_i(\omega_{r,i}) z_i \\ -\Gamma_i(\omega_{r,i}, V_{r_i}) \Theta_i(\omega_{r,i}) z_i \\ 1 \\ -\alpha_i K_c \sum_{j=1}^{N} \alpha_j (\Psi_{r,i} - \Psi_{r,j}) + K_e \tilde{\Psi}_i \end{bmatrix} \tag{9}$$

$$G_i := \begin{bmatrix} \xi_{1,i}^\top & \tilde{x}_i & z_i & h_i(\xi_i) & 0 & \Psi_{r,i} \end{bmatrix}^\top \tag{10}$$

such that, $f_i, G_i \in \mathbb{H}_i \times [0,1]^N$ with $\mathbb{H}_i := \mathbb{R}^8 \times [0,T]$. $\alpha_i = 1$ represents that the battery i is connected to the PCC or in discharging mode and $\alpha_i = 0$ otherwise.

$$h_i(\xi_i) := (\underset{i\in\mathbb{K}}{\text{argmin}}\, \tilde{x}_i^\top P_{L,i} \alpha_i (A_i \tilde{x}_i + B_i (u_i - \Gamma_i(\omega_{r,i}, V_{r_i}) z_i))) - \Gamma_i(\omega_{r,i}, V_{r_i}) z_i$$

and, finally, for any $P_{L,i}, Q_{L,i} \in \mathbb{R}^{2\times 2} \succ 0$ that satisfy Assumption 1,

$$\mathcal{C}_i := \{(\xi_{1,i}, \xi_{2,i}) \in \mathbb{H}_i : \tilde{x}_i^\top P_{L,i} (A_i \tilde{x}_i + B_i v_i) \leq -\eta_i \tilde{x}_i^\top Q_{L,i} \tilde{x}_i\} \cup \{(\xi_{1,i}, \xi_{2,i}) \in \mathbb{H}_i : \tau_i \in [0,T]\} \tag{11}$$

$$\mathcal{D}_i := \{(\xi_{1,i}, \xi_{2,i}) \in \mathbb{H}_i : \tilde{x}_i^\top P_{L,i} (A_i \tilde{x}_i + B_i v_i) \geq -\eta_i \tilde{x}_i^\top Q_{L,i} \tilde{x}_i\} \cap \{(\xi_{1,i}, \xi_{2,i}) \in \mathbb{H}_i : \tau_i = T\}. \tag{12}$$

$\eta_i \in (0,1)$ according to [15]. Note that v_i and τ_i change their values once that a minimum dwell-time, T, has elapsed and condition $\tilde{x}_i^\top P_{L,i} (A_i \tilde{x}_i + B_i v_i) \geq -\eta_i \tilde{x}_i^\top Q_{L,i} \tilde{x}_i$ is verified.

Note that (6) is obtained from easy mathematical manipulations of $\xi_{1,i}$ dynamic. The dynamic of $\xi_{2,i}$ comes from [15] and is presented in Section II-A. Finally, the $\Psi_{r,i}$ dynamic is given in (5).

Consider a predefined parameter $X_i > 0$, then

$$\mathcal{A}_i := \{\xi_i \in \mathbb{H}_i \times [0,1] : \|\tilde{x}_i\| < X_i, \xi_{1,i} = \mathbf{0}, \Psi_{r,i} = \Psi^*\} \tag{13}$$

is here the attractor associated with hybrid system $\mathcal{H}_i$, which is inspired by [15]. Ψ^* is a consensus value between all connected $\Psi_{r,i}$.

A. Global hybrid structure

We need to define a compact hybrid dynamical system that collects all dynamics $i \in \mathcal{N}$ with the aim at providing a large-signal analysis stability of the complete system. Previously to this model, a Laplacian matrix definition is given.

Definition 1: Consider a network defined by a undirected graph $\mathcal{G}(\mathcal{N}, \mathcal{E})$, being $\mathcal{N}$ the set of batteries in

discharging mode, and $\mathcal{E} \subseteq \mathcal{N} \times \mathcal{N}$ the edges. The Laplacian matrix that represents the interconnections between the neighbors of $\mathcal{G}$ is $L(\alpha) := \Delta(\alpha) - \mathcal{A}_d(\alpha)$, being $\alpha := \text{diag}\{\alpha_1, \alpha_2, .., \alpha_N\}$, $\Delta(\alpha) = \underset{i\in\mathcal{N}}{\text{diag}}\{\sum_{j\in\mathcal{N}, j\neq i} \alpha_{ij} := \alpha_i\alpha_j)\}$ and $\mathcal{A}_d(\alpha)$ the adjacency matrix $\mathcal{A}_d(\alpha) = [a_{ij}(\alpha)]$, where

$$a_{ij}(\alpha) : \begin{cases} \alpha_{ij} & \text{if} \quad i \neq j \text{ and } \forall (i,j) \in \mathcal{E} \\ 0 & \text{if} \quad i = j \text{ or } \forall (i,j) \notin \mathcal{E}. \end{cases} \tag{14}$$

The Laplacian matrix $L(\alpha)$ is positive semi-definite [18].

Now, we can formulate the compact hybrid system:

$$\mathcal{H}(\xi) : \begin{cases} \dot{\xi} = f(\xi) & \xi \in \mathcal{C} \\ \xi^+ \in G(\xi) & \xi \in \mathcal{D}, \end{cases} \tag{15}$$

$$f(\xi) := \begin{bmatrix} -K_\omega\tilde{\omega} - K_1\tilde{\Psi} \\ -K_\Psi\tilde{\Psi} + K_1\tilde{\omega} + K_0\tilde{P} \\ -K_P\tilde{P} - K_0\tilde{\Psi} \\ A\tilde{x} + Bv \\ \Theta(\omega_r)z \\ -\Gamma(\omega_r, V_r)\Theta(\omega_r)z \\ 1 \\ -K_cL(\alpha)\Psi_r + K_e\tilde{\Psi} \end{bmatrix} \tag{16}$$

$$G(\xi) \in \bigcup_{i\in\mathcal{N}} G_i(\xi_i) \tag{17}$$

with $\tilde{\Psi} := \underset{i\in\mathcal{N}}{\text{col}}\{\tilde{\Psi}_i\}$, $\tilde{\omega} := \underset{i\in\mathcal{N}}{\text{col}}\{\tilde{\omega}_i\}$, $\tilde{P} := \underset{i\in\mathcal{N}}{\text{col}}\{\tilde{P}_i\}$, $\tilde{x} := \underset{i\in\mathcal{N}}{\text{col}}\{x_i\}$, $v := \underset{i\in\mathcal{N}}{\text{col}}\{v_i\}$, $z := \underset{i\in\mathcal{N}}{\text{col}}\{z_i\}$, $\tau := \underset{i\in\mathcal{N}}{\text{col}}\{\tau_i\}$, $B := \underset{i\in\mathcal{N}}{\text{col}}\{\alpha_i B_i\}$, $A := \underset{i\in\mathcal{N}}{\text{diag}}\{\alpha_i A_i\}$, $\Theta := \underset{i\in\mathcal{N}}{\text{diag}}\{\Theta_i\}$, $\Gamma := \underset{i\in\mathcal{N}}{\text{diag}}\{\Gamma_i\}$, $\xi_1 := [\tilde{\omega}, \tilde{\Psi}, \tilde{P}]^\top$, $\xi_2 := [\tilde{x}, z, v, \tau]^\top$, $\xi := [\xi_1^\top, \xi_2^\top, \Psi_r]^\top$ and

$$\mathcal{C} = \prod_{i\in\mathcal{N}} \mathcal{C}_i \times [0,1]^N, \qquad \mathcal{D} = \prod_{i\in\mathcal{N}} \mathcal{D}_i \times [0,1]^N. \tag{18}$$

For large signal analysis purpose, we need to guarantee three time-scale separation to apply singular perturbation theory on hybrid dynamical systems [19], between ξ_1, ξ_2 and Ψ_r. To do so, next assumption must be satisfied.

Assumption 2: Consider (15)–(18). Then, there exist some parameters T, $K_c >> K_e > 0$, $K_0, K_1, K_\omega, K_\Psi, K_P > 0$, $K_{dc} := \underset{i\in\mathcal{N}}{\min}(\min|\text{Re}(\text{eig}(\mathbf{K}))|)$ with $\mathbf{K} := \begin{bmatrix} -K_\omega & -K_1 & 0 \\ K_1 & -K_\Psi & K_0 \\ 0 & -K_0 & -K_P \end{bmatrix}$, and $K_{inv} := \underset{i\in\mathcal{N}}{\min}(\min|\text{Re}(\text{eig}(A_i))|)$ such that

1) $K_c >> \frac{1}{T} >> K_{inv}$
2) $K_c >> K_{inv} >> K_{dc}$

are satisfied.

Note that $\frac{1}{K_c}, \frac{1}{K_{inv}}, \frac{1}{K_{dc}}$ represent the estimations of the convergence speed of each control loop. Then, this assumption implies that Ψ_r is faster than ξ_2, because $\frac{1}{K_c} << \frac{1}{K_{inv}}$ and, that ξ_2 is faster than ξ_1, because $\frac{1}{K_{inv}} << \frac{1}{K_{dc}}$.

IV. STABILITY CONDITIONS

Inspired in [20], we provide here a large-signal stability analysis for islanded AC microgrid. To do so, we assume that Assumption 2 is satisfied such that we define the next singular perturbation form for $\mathcal{H}$.

$$\mathcal{H}_{sp}(\xi) : \begin{cases} \begin{bmatrix} \dot{\xi}_1 \\ \dot{\xi}_2 \\ \nu\dot{\Psi}_r \end{bmatrix} = f_{sp}(\xi) & \xi \in \mathcal{C}, \\ \xi^+ \in G(\xi) & \xi \in \mathcal{D}, \end{cases} \tag{19}$$

such that

$$f_{sp}(\xi) := \begin{bmatrix} -K_\omega\tilde{\omega} - K_1\tilde{\Psi} \\ -K_\Psi\tilde{\Psi} + K_1\tilde{\omega} + K_0\tilde{P} \\ -K_P\tilde{P} - K_0\tilde{\Psi} \\ A\tilde{x} + Bv \\ \Theta(\omega_r)z \\ -\Gamma(\omega_r, V_r)\Theta(\omega_r)z \\ 1 \\ -L(\alpha)\Psi_r + \nu K_e\tilde{\Psi} \end{bmatrix} \tag{20}$$

with $\nu := 1/K_c$. Note that G does not change in this singular perturbation form w.r.t. the original scheme $\mathcal{H}$.

Now, the goal is to prove Semi-Global Practical Stability (SPAS) of set $\mathcal{A} := \prod_{i\in\mathcal{N}} \mathcal{A}_i$ if ν tends to 0^+. To do so, we introduce the next propositions:

Proposition 1: System $\mathcal{H}_{sp}(f_{sp}, G, \mathcal{C}, \mathcal{D})$ has the property to be well-posed.

Proof: $\mathcal{H}_{sp}(f_{sp}, G, \mathcal{C}, \mathcal{D})$ verifies the following properties [14, Section 6.2]

- each $[0,1] \subset \mathbb{R}$ given in (18) is a compact set.
- $\mathcal{C}_i, \mathcal{D}_i \in \mathbb{H}_i$ given in (18) present the characteristic to be closed sets;
- f_{sp} is a continuous function, thus outer semi-continuous and locally bounded. Moreover, for $\xi \in \mathcal{C}$, f_{sp} is convex and nonempty;
- G is locally bounded and outer semi-continuous. In addition, for $\xi \in \mathcal{D}$, G is nonempty;

Then, from [14, Section 6.2] is hold that $\mathcal{H}_{sp}$ is well posed. ■

Proposition 2: Consider Assumption 2 is satisfied. The quasi-steady-state equilibrium of $\mathcal{H}_{sp}$ is regular.

Proof: If Assumption 2 is satisfied, then $K_e << K_c$. As $\nu^+ \to 0$, $\nu K_e\tilde{\Psi} \to 0$ being

$$L(\alpha)\Psi_r = \begin{cases} 0 & \xi_i \in \mathcal{C}_i \\ \emptyset & \xi_i \notin \mathcal{C}_i \end{cases}$$

the quasi-steady-state equilibrium of $\mathcal{H}_{sp}$. ■

Proposition 3: Consider Assumption 2 is satisfied. The compact set

$$\mathcal{M} := \{\xi : (\xi_1, \xi_2) \in \mathcal{C} \cap \{L(\alpha)\Psi_r = \mathbf{0}\}, L(\alpha)\Psi_r = \mathbf{0}\}$$

associated to the *boundary layer* of $\mathcal{H}_{sp}$

$$\begin{bmatrix} \dot{\xi}_1 \\ \dot{\xi}_2 \\ \nu\dot{\Psi}_r \end{bmatrix} = \begin{bmatrix} \mathbf{0} \\ \mathbf{0} \\ -L(\alpha)\Psi_r \end{bmatrix} \tag{21}$$

is Globally Asymptotically Stable (GAS).

Proof: First note that if Assumption 2 is satisfied ($K_e << K_c$), then the flow dynamic (21) is straightforward, re-scaling the ordinary time, t by $1/\nu$, in (19) and doing $\nu = 0$. Moreover, we stress that there is not jump in the boundary layer, remaining ξ_1 and ξ_2 constant during flows.

Now, consider the Lyapunov function candidate

$$V_c := \frac{1}{2}{\Psi_r}^\top L(\alpha)\Psi_r.$$

Then, $\langle \nabla V_c(\Psi_r), f_{bl}\rangle = -{\Psi_r}^\top L(\alpha)L(\alpha)\Psi_r \leq 0$, being $f_{bl} := [\mathbf{0}^\top \ \mathbf{0}^\top \ -\Psi_r^\top L(\alpha)]^\top$. Note that $\langle \nabla V_c(\Psi_r), f_{bl}\rangle$ is negative semidefinite. Indeed, the control law defined in the dynamic Ψ_r guarantees that each $\Psi_{r,i}$ with associated $\alpha_i = 1$ converges to a neighborhood of $\Psi^* = \frac{\mathbf{1}^\top\alpha\Psi_r}{\mathbf{1}^\top\alpha\mathbf{1}}$ if $\mathbf{1}^\top\alpha\mathbf{1} \neq 0$. Consequently, $\mathcal{M}$ is GAS for (21). ∎

Proposition 4: Consider Assumptions 1, 2 are satisfied. The attractor $\mathcal{A}_r := \prod_{i\in\mathcal{N}} \mathcal{A}_{r,i}$ with $\mathcal{A}_{r,i} := \{\xi_i \in \mathbb{H}_i \times [0,1] : \|\tilde{x}_i\| < X_i, \xi_{1,i} = \mathbf{0}\}$

associated to the reduced system:

$$\mathcal{H}_r(\xi):\begin{cases} \left[\begin{array}{c} \dot{\xi}_1 \\ \hline \\ \dot{\xi}_2 \end{array}\right] = \left[\begin{array}{c} -K_\omega\tilde{\omega} - K_1\tilde{\Psi} \\ -K_\Psi\tilde{\Psi} + K_1\tilde{\omega} + K_0\tilde{P} \\ -K_P\tilde{P} - K_0\tilde{\Psi} \\ \hline A\tilde{x} + Bv \\ \Theta_i(\omega_r, V_r)z \\ -\Gamma(\omega_r, V_r)\Theta(\omega_r)z \\ 1 \end{array}\right] & \xi \in \mathcal{C}_H \\ \begin{bmatrix} \xi_1^+ \\ \xi_2^+ \end{bmatrix} \in \bigcup_{i\in\mathcal{N}} G_{r,i}(\xi_{1,i}, \xi_{2,i}) & \xi \in \mathcal{D}, \end{cases} \tag{22}$$

being $\mathcal{C}_H := \mathcal{C} \cap \{L(\alpha)\Psi_{r,i} = \mathbf{0}\}$ and $G_{r,i}(\xi_{1,i}, \xi_{2,i}) := \begin{bmatrix}\xi_{1,i}^\top & \tilde{x}_i^\top & z_i & h_i(\xi_i) & 0\end{bmatrix}^\top$ is Uniformly Globally Asymptotically Stable (UGAS).

Proof: Note that we have here a cascade system composed of the control inverter which is faster enough than the droop control. Then, consider the following Lyapunov function for the reduced system $\mathcal{H}_r$,

$$V(\xi_1, \tilde{x}) := \sum_{i\in\mathcal{N}} V_i(\xi_{1,i}, \tilde{x}_i)$$
$$V_i(\xi_{1,i}, \tilde{x}_i) = \frac{1}{2}(\xi_{1,i}^\top\xi_{1,i} + \tilde{x}_i^\top P_{L,i}\tilde{x}_i).$$

Applying [15, Theorem 1] to hybrid system $\mathcal{H}_r$, it is got

$$\langle \nabla V_i(\xi_{1,i}, \tilde{x}_i)\rangle = -\xi_{1,i}^\top S\xi_{1,i} + \alpha_i\tilde{x}_i P_{L,i}(A_i\tilde{x}_i + B_i v_i)$$
$$\leq -\xi_{1,i}^\top S\xi_{1,i} - \alpha_i\eta_i\tilde{x}_i^\top Q_{L,i}\tilde{x}_i < 0 \tag{23}$$
$$V_i(\xi_{1,i}^+, \tilde{x}_i^+) - V_i(\xi_{1,i}, \tilde{x}_i) = 0 \tag{24}$$

with $S := \text{diag}\{K_\omega, K_\Psi, K_P\}$.

If Assumption 1 is satisfied and from [15, Theorem 1 and 2], we can conclude that $\mathcal{A}_{r,i}$ is UGAS. ∎

Theorem 1: For a given $Q_{L,i} \in \mathbb{R}^{n\times n} \succ 0$, there exists any $P_{L,i} \in \mathbb{R}^{n\times n} \succ 0$ that satisfies Assumption 1 for each $i \in \mathcal{N}$. Moreover, for some selected parameters $T, K_\omega, K_\Psi, K, K_0, K_1, K_c, K_e > 0$ satisfying Assumption 2 and a given interconnected graph, $\mathcal{G}(\mathcal{N}, \mathcal{E})$, $\mathcal{A}$ is SPAS for hybrid system $\mathcal{H}$, (15)–(18). □

Proof: The proof is direct from Proposition 1–4 and the proof of [19, Theorem 1]. ∎

V. SIMULATION RESULTS

The hybrid control proposed here is validated in Matlab/Simulink by using the Electrical Toolbox for an AC-bus microgrid composed by 3 batteries in discharging mode. A similar scenario was given in [3]. The bus line voltage is $V_{bus} = 120\sqrt{2}\sin(2\pi 60t)V = V_n sin(\omega_n t)$. $P_{L,i} = \begin{bmatrix}28.20 & 0.12 \\ 0.12 & 0.08\end{bmatrix}$ and $Q_{L,i} = \begin{bmatrix}1.50 & 0 \\ 0 & 5.55\end{bmatrix}$ satisfy Assumption 1 and $X_i = 0.041$. Finally, Table I and II provide the parameters for the secondary and primary control loop respectively, i.e., the parameters for the hybrid model (9)–(12). From these parameters, we have $K_e/K_c = 0.01$, $K_{inv} = 34.7$ and $K_{dc} = 0.51$, then it is easy to see that Assumption 2 is satisfied.

TABLE I

MICROGRID AND DROOP CONTROL PARAMETERS

Parameter	Value	Parameter	Value
K_c	10000	K_P	50
K_e	100	K_1	0.5
K_Ψ	0.45	K_0	0.05
K_ω	5		

TABLE II

INVERTER PARAMETERS

Parameter $\forall i$	Value	Parameter $\forall i$	Value
$V_{in,i}$	48V	ω_n	60Hz
L_i	50mH	V_n	$120\sqrt{2}$V
C_i	140.72μF	$\delta_{k,i}$	$6.12W/h$
$R_{LS,i}$	1.5Ω	T	0.1ms
R_i	180Ω		

We consider that at the instant time $T_2 = 1.5$s the battery 1 is disconnected, and then it is connected back in $T_3 = 1.7$s. Also at $T_1 = 0.5$s a communication failure occurs between battery 1 and 3, i.e., $\alpha_{1,3} = 0$. We consider that the net power (load power minus DG power) is $P_n = 300$W. Fig. 2 shows the convergence of the SOC reference, $\Psi_{r,i}$, to a consensus from the initial conditions and after the battery plug-and-play event. Note that the transient times are less than 0.1μs. The estimated SOCs and active powers converge to their references approximately before to 2s. Moreover, note that the signals evolve robustly after the communication failure. In Fig. 3 the voltage reference errors are shown. Note that these errors present a transient time less than 30ms. Finally, Fig 4 shows the voltages, currents, and duty cycles. Note as these inverters evolve slower than the SOC references to a consensus and, faster than the droop control, validating the time-scale separation assumption.

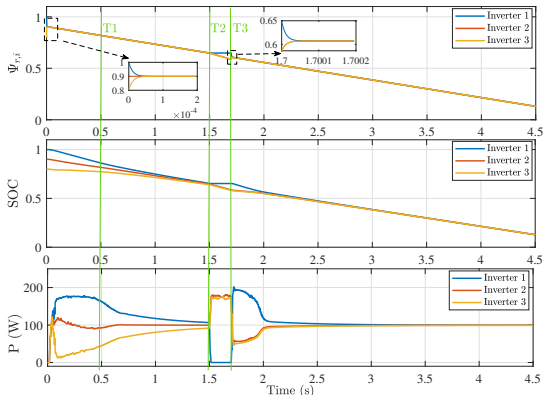

Fig. 2. Evolution of $\Psi_{r,i}$, Ψ_i, and the active powers P_i, for $i = \{1, 2, 3\}$, when the battery 1 is disconnected at T_2 and then connected back at T_3. In T_1, $\alpha_{1,3}$ turns to 0.

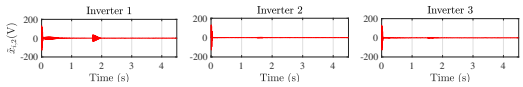

Fig. 3. Evolution of the voltage errors.

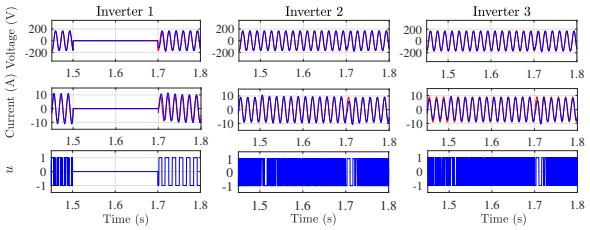

Fig. 4. Evolution of the voltages, currents and duty cycles of inverters between 1.45s to 1.8s.

Indeed, we highlight that $1/K_d = 2$, $1/K_{inv} = 28ms$ and $1/K_c = 0.1\mu s$. Note again they are robust w.r.t the communication failure. From this simulation, we can validate Theorem 1 statement.

VI. CONCLUSION

This work provides a complete hybrid scheme for the primary and secondary control loops in an islanded AC-bus microgrid. The scheme considers nonlinearities in the inverter model (switching and affine terms) and in the signals (minimum-dwell time constraint). Moreover, the secondary loop is composed of a consensus algorithm connected to a droop control to increase the battery lifespan, as well as provide robustness with respect to a plug-and-play event or any communication failure. The scalability of the microgrid is also a characteristic ensured with the proposed algorithm. A large-signal stability analysis for the inverter control, droop control, and consensus algorithm is obtained by applying singular perturbation theory to a time-scale separation hybrid model obtained by selecting the controller gains appropriately. Then, it is concluded that the attractor $\mathcal{A}$ is SPAS. As a future work, experimental results are expected to be performed to validate the SOC consensus convergence. It is also envisioned to extend these results adding an extra control loop to manage the functioning mode of the batteries, loads and/or sources (*charging mode or discharging mode*) to improve the battery degradations.

REFERENCES

[1] R. H. Lasseter and P. Paigi, "Microgrid: A conceptual solution," in IEEE 35th annual power electronics specialists conference, vol. 6, 2004, pp. 4285–4290.

[2] T. Caldognetto, P. Tenti, A. Costabeber, and P. Mattavelli, "Improving microgrid performance by cooperative control of distributed energy sources," IEEE Trans. Ind. Appl., vol. 50, no. 6, pp. 3921–3930, 2014.

[3] C. Li, E. Coelho, T. Dragicevic, J. Guerrero, and J. Vasquez, "Multiagent-based distributed state of charge balancing control for distributed energy storage units in AC microgrids," IEEE Trans. Ind. Appl., vol. 53, no. 3, pp. 2369–2381, 2016.

[4] O. Palizban and K. Kauhaniemi, "Power sharing for distributed energy storage systems in AC microgrid: Based on state-of-charge," pp. 1–5, 2015.

[5] T. Morstyn, A. V. Savkin, B. Hredzak, and V. Agelidis, "Multi-agent sliding mode control for state of charge balancing between battery energy storage systems distributed in a DC microgrid," IEEE Trans. Smart Grid, vol. 9, no. 5, pp. 4735–4743, 2017.

[6] D. Li, Z. Wu, B. Zhao, and L. Zhang, "An improved droop control for balancing state of charge of battery energy storage systems in AC microgrid," IEEE Access, vol. 8, pp. 71 917–71 929, 2020.

[7] Y. Guan, L. Meng, C. Li, J. Vasquez, and J. Guerrero, "A dynamic consensus algorithm to adjust virtual impedance loops for discharge rate balancing of AC microgrid energy storage units," IEEE Trans. Smart Grid, vol. 9, no. 5, pp. 4847–4860, 2017.

[8] R. Zhang and B. Hredzak, "Nonlinear sliding mode and distributed control of battery energy storage and photovoltaic systems in AC microgrids with communication delays," IEEE Trans. Industr. Inform., vol. 15, no. 9, pp. 5149–5160, 2019.

[9] M. Kabalan, P. Singh, and D. Niebur, "Large signal lyapunov-based stability studies in microgrids: A review," IEEE Trans. Smart Grid, vol. 8, no. 5, pp. 2287–2295, 2016.

[10] W. Xie, M. Han, W. Cao, J. Guerrero, and J. Vasquez, "System-level large-signal stability analysis of droop-controlled DC microgrids," IEEE Trans. Power Electron., vol. 36, no. 4, pp. 4224–4236, 2020.

[11] Y. Xia, Z. Lv, W. Wei, and H. He, "Large-signal stability analysis and control for small-scale AC microgrids with single storage," IEEE Trans. Emerg. Sel, vol. 10, no. 4, pp. 4809–4820, 2021.

[12] M. Farokhian Firuzi, A. Roosta, and M. Gitizadeh, "Stability analysis and decentralized control of inverter-based AC microgrid," Prot. Control Mod. Power Syst., vol. 4, no. 1, pp. 1–24, 2019.

[13] R. Goebel, R. Sanfelice, and A. Teel, "Hybrid dynamical systems," IEEE Control Syst., vol. 29, no. 2, pp. 28–93, 2009.

[14] R. Goedel, R. Sanfelice, and A. Teel, "Hybrid dynamical systems: modeling stability, and robustness," Princeton, NJ, USA, 2012.

[15] C. Albea, O. Lopez Santos, D. Zambrano Prada, F. Gordillo, and G. Garcia, "On the practical stability of hybrid control algorithm with minimum dwell time for a DC-AC converter," IEEE Trans. Control Syst. Technol., 2018.

[16] C. Albea and G. Garcia, "Robust hybrid control law for a boost inverter," Control. Eng. Pract., vol. 101, p. 104492, 2020.

[17] G. S. Deaecto, J. C. Geromel, F. Garcia, and J. Pomilio, "Switched affine systems control design with application to DC–DC converters," IET Control. Theory Appl., vol. 4, no. 7, pp. 1201–1210, 2010.

[18] R. Olfati-Saber and R. Murray, "Graph rigidity and distributed formation stabilization of multi-vehicle systems," in Proc. IEEE Conf. Decis. Control., vol. 3, 2002, pp. 2965–2971.

[19] R. Sanfelice and A. Teel, "On singular perturbations due to fast actuators in hybrid control systems," Automatica, vol. 47, no. 4, pp. 692–701, 2011.

[20] C. Albea, "Hybrid dynamical control based on consensus algorithms for current sharing in DC-bus microgrids," Nonlinear Anal.: Hybrid Syst., vol. 39, p. 100972, 2021.